J Mater Sci (2013) 48:5280–5286
DOI 10.1007/s10853-013-7319-4

The role of iron in the formation of inorganic polymers (geopolymers) from volcanic ash: a ^{57}Fe Mössbauer spectroscopy study

Patrick N. Lemougna · Kenneth J. D. MacKenzie · Guy N. L. Jameson · H. Rahier · U. F. Chinje Melo

Received: 15 January 2013 / Accepted: 12 March 2013 / Published online: 20 March 2013

Abstract The behavior of the iron present in two volcanic ashes was investigated during geopolymer synthesis using sodium hydroxide as the sole alkali activator. XRD, SEM, and room-temperature ^{57}Fe Mössbauer spectroscopy were used to monitor the behavior of the iron during the synthesis reaction. Geopolymers with very good compressive strengths were formed, especially with the finer ash, in which the iron is present in the crystalline minerals ferroan forsterite and augite. Mössbauer spectroscopy identified the ferrous sites in these minerals, plus a ferric site, probably located in an X-ray amorphous phase. The ferroan forsterite in the original ashes did not react with NaOH, but a substantial proportion of the augite reacted to form new ferric sites with parameters similar to distorted tetrahedral or 5-coordinated environments, suggesting the possible incorporation of ferric iron in the tetrahedral network of the geopolymer product. These results indicate that iron is not necessarily deleterious to geopolymer formation, as has sometimes been suggested.

P. N. Lemougna · U. F. Chinje Melo
Physico-Chemistry of Mineral Materials Laboratory, University of Yaoundé I, and Local Materials Promotion Authority, MINRESI/MIPROMALO, P.O. Box 2396, Yaounde, Cameroon

K. J. D. MacKenzie (✉)
MacDiarmid Institute for Advanced Materials and Nanotechnology, School of Chemical and Physical Sciences, Victoria University of Wellington, Wellington, New Zealand
e-mail: kenneth.mackenzie@vuw.ac.nz

G. N. L. Jameson
Department of Chemistry & MacDiarmid Institute for Advanced Materials and Nanotechnology, University of Otago, Dunedin, New Zealand

H. Rahier
Department of Materials and Chemistry, Vrije Universiteit Brussel, Pleinlaan 2, 1050 Brussel, Belgium

Introduction

Alternative low-energy materials such as inorganic polymers (geopolymers) produced from natural minerals or inorganic wastes have attracted interest in the last three decades as possible more ecologically friendly cementitious materials [1–4]. Geopolymers consist of tetrahedral aluminate and silicate units linked by oxygen atoms, the negative charge of Al^{3+} in fourfold coordination being compensated by ions such as Na^+, K^+, Li^+, and Cs^+ [5–8].

Despite the large number of research papers reported on geopolymer chemistry, some aspects of the synthesis mechanisms are still not well understood. Competing reactions as well as the role played by the impurities present in natural aluminosilicate raw materials remain largely elusive [9, 10]. Among these impurities, iron species are of particular interest since iron is the most abundant crustal transition metal, accounting for 6 % of the chemical composition of the Earth's crust [11]. This element is also commonly found in varying amounts in many aluminosilicate materials (fly ashes, volcanic ashes, and metakaolin derived from low-purity natural kaolin) of potential use as raw materials for geopolymer synthesis [12–19]. So far, the few investigations carried out on the role of iron in geopolymerization have led to some controversies, probably linked to the nature of the initial components in the geopolymer mixtures [13, 15–19]. The possible implication of iron in the geopolymerization of natural volcanic ash has previously been reported [13, 20]. However, these reports were limited to the determination of their amount in the starting ashes, and provided no information on the role played by iron in geopolymer formation.

In a study of a more carefully controlled model system, Perera et al. [18] prepared metakaolin-based geopolymers containing ferric solutions and showed by a combination of techniques including Mössbauer spectroscopy that the iron was present in octahedral sites, either as isolated ions or as unreacted oxyhydroxide aggregates. Bell and Kriven [21] attempted to produce iron analogs of conventional aluminosilicate geopolymers using synthetic iron silicate powder which proved far less reactive than metakaolinite, and formed a material containing predominantly octahedral iron that was unlike a conventional geopolymer.

The aim of the present work was to investigate the behavior of the iron in two volcanic ashes during alkali activation with NaOH. ^{57}Fe Mössbauer spectroscopy was used to monitor any changes in the iron valence and coordination number occurring during the geopolymerization process and the synthesized products were also characterized by X-ray diffraction (XRD), scanning electron microscopy (SEM), and compressive strength measurements.

Experimental

Materials

The two volcanic ashes (Va1 and Va2) used in this study were from Cameroon (from the Foumbot and Djoungo sites, respectively), situated in the west (Va1) and littoral (Va2) regions of Cameroon. The materials were ground to pass a 400-μm sieve. Their chemical composition, determined by X-ray fluorescence, is presented in Table 1 and their particle size distributions, determined by sieving–sedimentation, are listed in Table 2. The sodium hydroxide used for activation of the samples was of analytical grade (Merck).

Geopolymer synthesis

The inorganic polymer formulations were obtained by stirring the volcanic ash into an aqueous solution of NaOH prepared in distilled water. A series of mixtures was thus prepared with Na_2O/Al_2O_3 molar ratios ranging from 1.00 to 1.75 in 0.25 intervals, corresponding to initial NaOH solution concentrations from 8.3 to 19.1 M with 3.6 intervals and a water/ash ratio (weight) of 0.21 for both ashes at all the mixtures. This gave rise to the molar compositions shown in Table 3. The samples of all these compositions were used for compressive strength measurements, but the samples with $Na_2O/Al_2O_3 = 1.50$ were selected for XRD, SEM, and ^{57}Fe Mössbauer spectroscopy since these contained the highest Na content without being affected by the efflorescence that developed in the samples of higher Na content after a few days of exposure to the laboratory atmosphere. The mixed pastes were placed in 4 cm^2 polyethylene cubic molds and vibrated for 5 min to remove air bubbles. The molded samples were then cured at 40 °C for 2 days, then removed from the molds, and dried at 90 °C for 5 days.

Table 2 Particle size analysis of the ash samples

Sample	100–400 μm	2–100 μm	<2 μm
Va1	12 %	81 %	7 %
Va2	52 %	41 %	7 %

Product characterization

Room-temperature ^{57}Fe Mössbauer spectra of the samples before and after alkali activation were recorded at the University of Otago on a Mössbauer spectrometer from SEE Co. (Science Engineering & Education Co., MN).

About 100 mg of sample was placed in a nylon sample holder (12.8 mm diameter, 1.6 mm thickness) with Kapton windows. Data were collected in constant acceleration mode in transmission geometry with an applied field of 47 mT parallel to the γ-rays. The zero velocity of the Mössbauer spectra refers to the centroid of the room-temperature spectrum of a 25-μm metallic iron foil. Analysis of the spectra was conducted using the WMOSS program (SEE Co, formerly WEB Research Co. Edina, MN).

X-ray diffraction was carried out on powdered samples using a Philips PW1700 computer-controlled diffractometer with a graphite monochromator and Co Kα radiation. The XRD traces were measured from 4° to 80° 2θ at a 0.04° 2θ step size, 4 s/step.

Scanning electron micrographs with secondary electron imaging and elemental mapping were carried out on polished samples coated with about 20 nm of carbon using a Jeol JSM 6400 microscope with an accelerating voltage of 20 kV.

The compressive strength of the samples (4 × 4 × 4 cm^3 size) was measured with an Instron 5885 H Compression machine with a displacement speed of 0.5 mm/min. The results shown here are averages of three replicate specimens.

Table 1 Chemical analysis of the ash samples (wt%)

Sample	SiO_2	Al_2O_3	Fe_2O_3	CaO	MgO	Na_2O	K_2O	TiO_2	P_2O_5	MnO	SUM
Va1	43.4	15.3	12.5	11.1	6.8	4.5	1.7	2.9	0.9	0.2	99.4
Va2	43.4	15.1	13.8	11.2	5.8	4.1	1.8	3.3	0.9	0.2	99.5

Table 3 Molar compositions of the geopolymer samples

Ash	SiO_2:Al_2O_3	Na_2O:SiO_2	Na_2O:Al_2O_3	Na_2O:(Al_2O_3 + Fe_2O_3)	H_2O:Na_2O
Va1	4.81	0.20	1.0	0.64	7.93
Va1	4.81	0.26	1.25	0.80	6.32
Va1	4.81	0.31	1.5	0.97	5.25
Va1	4.81	0.36	1.75	1.14	4.49
Va2	4.86	0.20	1.0	0.62	7.93
Va2	4.86	0.26	1.25	0.78	6.32
Va2	4.86	0.31	1.5	0.95	5.25
Va2	4.86	0.36	1.75	1.11	4.49

Results and discussion

X-ray diffraction

The X-ray diffractograms of the two samples before and after alkali activation at a Na_2O/Al_2O_3 molar ratio of 1.50 (Fig. 1) are quite similar, containing a mixture of amorphous and crystalline phases. The XRD traces indicate that the iron is present as Fe(II) in the minerals: augite, $(CaMg_{0.74}Fe_{0.25})Si_2O_6$ (JCPDF file no 01-070-3753), and ferroan forsterite, $(Mg_{0.9}\ Fe_{0.1})2SiO_4$ (JCPDF file no 01-076-0513). Augites are also known to contain small amounts of Fe(III) [22], but it is likely that if any iron of this valency is present, it would occur mainly in the poorly crystallized regions, in light of the percentage of trivalent Fe indicated by Mössbauer spectroscopy (see below).

It is also observed that the intensity ratio of the peaks from the augite mineral is greater than that of ferroan forsterite. As the patterns were not scaled to a specific peak, this suggests that augite is the predominant iron-containing crystalline phase in the ashes.

Other crystalline minerals shown by XRD to be present are disordered sodian anorthite, $(Ca,Na)(Si,Al)_4O_8$ (JCPDF file no 00-041-1481), and, in the samples treated with NaOH, sodium aluminosilicate hydroxide hydrate, $Na_8(AlSiO_4)_6(OH)_2$-$4H_2O$ (JCPDS file no 00-041-0009). The presence of the latter suggests that some dissolved ash particles formed a crystalline phase. However, an amorphous component is present in both the untreated and alkali-activated ashes, as evidenced by the broad feature in the background at about 28°2θ, the intensity of this is essentially unchanged after the formation of the geopolymer supporting the premise that the major reaction product is amorphous.

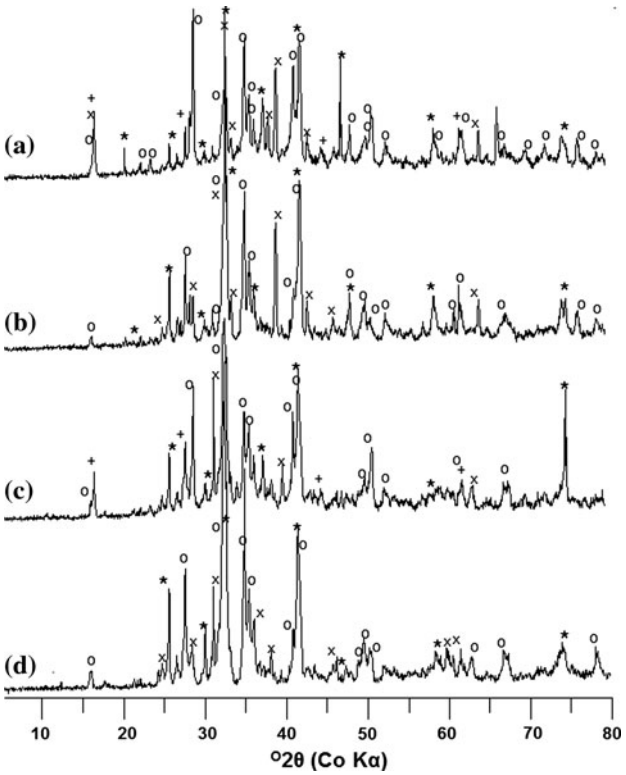

Fig. 1 XRD spectra of the initial ashes and the corresponding ashes alkali-activated at the molar composition $Na_2O/Al_2O_3 = 1.50$. **a** Va1 OH, **b** Va1, **c** Va2 OH, **d** Va2. *Key* * = augite, $(CaMg_{0.74}\ Fe_{0.25})Si_2O_6$ (JCPDS file no. 70-3753), o = ferroan forsterite, $(Mg_{0.9}\ Fe_{0.1})_2SiO_4$ (JCPDS File no. 76-0513), x = disordered sodian anorthite, $(Ca,Na)(Si,Al)_4O_8$ (JCPDS file no. 41-1481), + = sodium aluminosilicate hydroxide hydrate, $Na_8(AlSiO_4)_6(OH)_2$-$4H_2O$ (JCPDS file no. 41-0009). All the traces are scaled to the same number of counts

Scanning electron microscopy

SEM micrographs with EDS elemental mapping (Fig. 2) indicate a relatively homogeneous distribution of iron throughout both alkali-activated samples, with only a few small regions of higher iron content corresponding to less well-reacted iron minerals. The same phenomenon was observed for the Ca maps. By contrast, the Mg maps of the alkali-activated samples show regions of high magnesium content probably corresponding to the ferroan forsterite, suggesting that this is a less-reactive phase in the ash minerals. The behavior of Ca and Mg in the present volcanic ashes is in agreement with previous reports on alkali activation of fly ashes containing these elements [15].

Calcium was suggested to be active in the process of alkali activation of ash/slag blends, preferentially forming $Ca(OH)_2$ (which can be enclosed in the geopolymeric binder as it forms) rather than calcium (alumino) silicate hydrate or calcium aluminate hydrate phases [15–17]. The presence of Ca in the mixture during the formation of inorganic polymers was also suggested to significantly affect the setting time and the final properties depending on the concentration and the form of the additive [13, 17]. By contrast, Mg was found not to disperse into the gel to the same extent as Ca, probably due to the fact that when Mg is able to participate in the formation of hydrated silicate gel, the preference for this is much less strong than in the case of Ca [15]. On the other hand, iron was suggested to be less reactive during alkali activation of fly ash than calcium [15–17], and its widespread distribution observed by SEM was suggested to possibly arise from the occlusion by the glass of inert iron phases [15]. However, the same authors also suggested a possibility of differential solubility of iron phases, with a higher solubility for a few irons contained in the silicate-rich phases, which remained, however, difficult to be quantified by SEM [15]. A more in-depth study of the behavior of iron during alkali activation of the present volcanic ashes is presented in the Mössbauer spectroscopy section.

Compressive strength

Both the ash samples developed good compressive strengths (Fig. 3), although the samples derived from Va1 were significantly stronger at all concentrations of Na_2O. With the exception of Va2 at the lower alkali concentrations, these compressive strengths are superior to the strength of 25.1 MPa found for materials prepared by alkali activation of red mud [19] which contained a much higher concentration of Fe_2O_3 (42–50 wt%).

Attempts to produce iron geopolymers containing 100 % Fe [21] resulted in a water-soluble rubbery gel which partially hardened only after aging for 361 days in a closed container. The significantly lower Fe_2O_3 content of the present ashes (12 and 14 wt% in Va1 and Va2, respectively) (Table 1) is qualitatively consistent with the view that the presence of iron interferes with the development of strength, but the difference in iron content between Va1 and Va2 is insufficient to explain the much greater strength developed by the latter at all alkali concentrations. This suggests the operation of other factors such as the chemical and mineralogical form of the iron, the particle size distribution, and proportion of amorphous phases in the ashes which will influence their reactivity. Since the chemical and mineralogical compositions of both ashes are similar, the greater strength of the Va1 samples is most likely to arise from the greater reactivity of this ash resulting from its much higher content of particles in the range 2–100 μm (Table 2). Differences have also been observed in the heats of reaction of Va1 and Va2 with alkali concentration (unpublished results). The heat of reaction of Va2 increases with increasing Na content (from 40 J/g at Na_2O/Al_2O_3 of 1.00 to 80 J/g at Na_2O/Al_2O_3 of 1.75) as does the mechanical strength, but this is not the case for Va1 where only the reaction heat gradually increased with increasing Na content in the concentration range studied (from 70 J/g at Na_2O/Al_2O_3 of 1.00 to 110 J/g at Na_2O/Al_2O_3 of 1.75); this may again reflect differences in reactivity related to the particle size distribution of the ashes. The present compressive strengths (15–60 MPa) are similar to those of conventional metakaolin-based geopolymers containing Na and/or K alkali cations, in the Si/

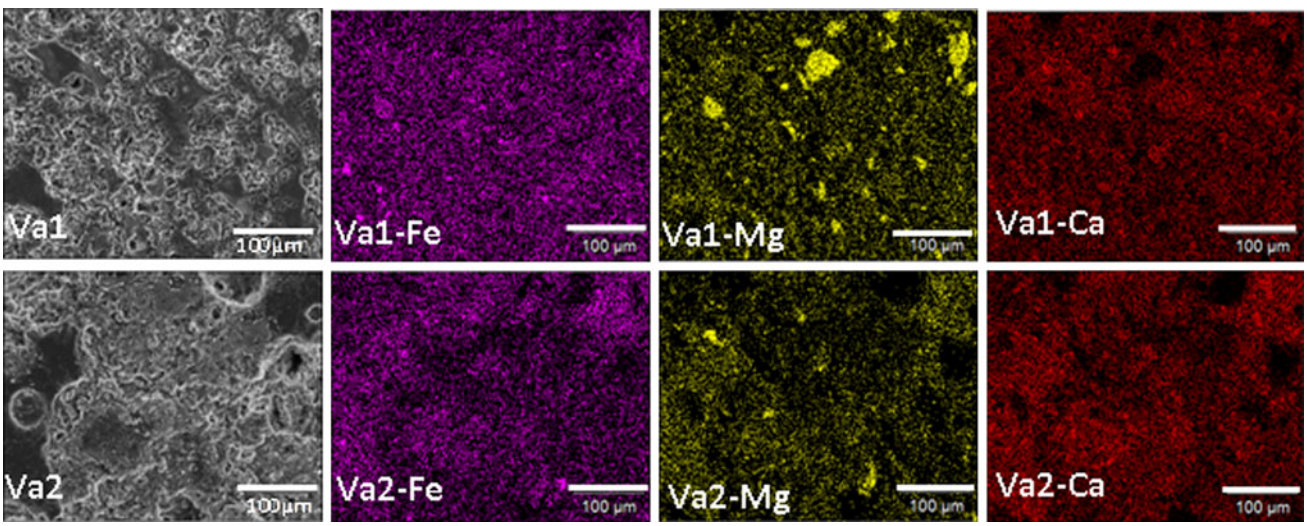

Fig. 2 SEM micrographs with EDS elemental mapping of Fe, Mg, and Ca of alkali-activated ashes at Na_2O/Al_2O_3 of 1.50

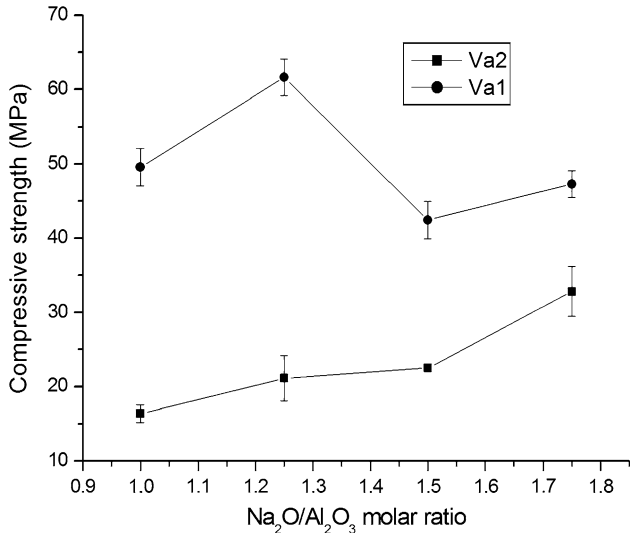

Fig. 3 Effect of the molar composition on the compressive strengths of the alkali-activated ashes

Al range 1.15–1.4 [23], indicating that although the effect of iron on the geopolymer-forming reaction is unclear at this stage, its presence in these concentrations does not militate against the development of adequate compressive strength.

Mössbauer spectroscopy

The ^{57}Fe Mössbauer spectra of the two ashes, before and after alkali activation, are shown in Fig. 4 and the corresponding Mössbauer parameters (quadrupole splitting (ΔEQ), isomer shift (δ), and line width ($\Gamma_{L\,=\,R}$)) are tabulated in Table 4. The spectra of both ashes before reaction with alkali are remarkably similar, and can be fitted to two Fe^{2+} quadrupole doublets and one Fe^{3+} doublet. Since both these ashes were shown by XRD to contain the two crystalline iron-bearing minerals ferroan forsterite and augite, the Mössbauer spectra should also reflect their presence. Ferroan forsterite is a member of the olivine group in which the Fe^{2+} is in octahedral coordination in two sites that are not always distinguished by Mössbauer spectroscopy [24]. The quadrupole splitting ΔEQ of site A in the present spectra is within the range of reported values for the olivines (2.80–3.02 mm s^{-1}) [24] and this assignment is also supported by the isomer shift δ which is close to the reported range (1.16–1.18 mm s^{-1}). By contrast, augite is a member of the pyroxene group, in which the single-stranded silicate chains are crosslinked by sixfold coordinated cations [24]. Since the quadrupole splitting is sensitive to the degree of distortion from octahedral symmetry, less distorted sites, as in forsterite, showing larger quadrupole splittings [25], the more distorted octahedral Fe^{2+} site with the smaller quadrupole splitting is assigned to augite; this is also consistent with the reported Mössbauer parameters for this group of minerals (ΔEQ = 1.91–2.69 mm s^{-1}, δ = 1.12–1.18 mm s^{-1}) [25]. The Fe^{2+} doublet B assigned to augite is also significantly broader than that of the ferroan forsterite doublet A (Table 4). Augite contains two sixfold coordinated Fe^{2+} sites which can, however, only be visually distinguished at much higher iron contents than in the present ashes [24] and the overlap of these two sites could explain the broadness of this doublet. The intensity ratios of these doublets are also very similar in unreacted Va1 and Va2 (Table 4), but the intensity of doublet B (augite) is more than twice that of doublet A (forsterite), suggesting that the former is the principal iron-containing species in these ashes. This is consistent with the XRD results (Fig. 1).

Both ashes contain a third doublet with Mössbauer parameters consistent with Fe^{3+} (ΔEQ = 0.89 mm s^{-1}, δ = 0.44 mm s^{-1}). Assignment of the ferric site to a particular phase is somewhat problematical. Ferric sites are known to exist in the silicate minerals of the garnet and epidote groups, but neither of these minerals were seen in the XRD traces, and their reported Mössbauer parameters [24] are significantly different from the present parameters. Recalculation of the precise formula of the present augite on the basis that these minerals are known to contain some Fe(III) to maintain electrical neutrality [22] results in the formula $CaMg_{0.74}Fe(II)_{0.23}$ $Fe(III)_{0.02}$, giving an atomic ratio FeIII/FeII of 0.086. This ratio is too small to explain

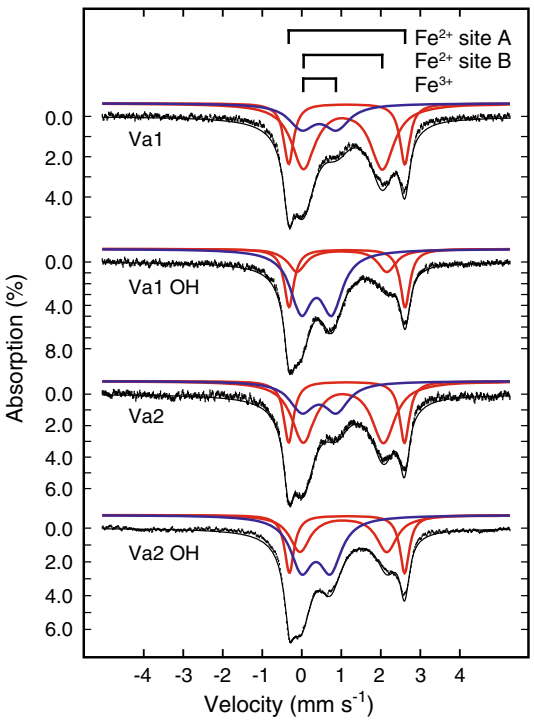

Fig. 4 Room-temperature Mössbauer spectra of the two ashes before alkali activation (Va1 and Va2) and after alkali activation (Va1 OH and Va2 OH)

Table 4 Mössbauer parameters (isomer shift δ, quadrupole splitting ΔE_Q, linewidth $\Gamma_{L=R}$, and intensity I) of the two ashes before alkali activation (Va1 and Va2) and after alkali activation (Va1OH and Va2 OH)

Sample	Species	δ (mm s^{-1})	ΔE_Q (mm s^{-1})	$\Gamma_{L=R}$ (mm s^{-1})	I (%)
Va1	Fe(II)A	1.14	2.94	0.31	23
Va1	Fe(II)B	1.04	2.00	0.73	55
Va1	Fe(III)	0.44	0.89	0.79	22
Va1 OH	Fe(II)A	1.15	2.94	0.30	24
Va1 OH	Fe(II)B	1.08	2.28	0.56	17
Va1 OH	Fe(III)	0.37	0.77	0.66	52
Va2	Fe(II)A	1.13	2.93	0.30	22
Va2	Fe(II)B	1.05	2.03	0.71	50
Va2	Fe(III)	0.44	0.88	0.74	25
Va2 OH	Fe(II)A	1.15	2.92	0.30	22
Va2 OH	Fe(II)B	1.05	2.20	0.63	29
Va2 OH	Fe(III)	0.36	0.73	0.68	44

the Fe(III) in the present Mössbauer spectra as arising from the augite. A further possibility is that the ferric iron resides in the amorphous phase shown to be present by the bulge in the background of the XRD traces. The absence of magnetic sextets in all of the spectra rules out most of the iron oxides and oxyhydroxides, although this is dependent on the size of the particles and temperature at which they were formed [26, 27]; this can lead to relaxation of the magnetic spectra, which depends on the temperature of the environment and may be the cause of relaxation here. A quadrupole doublet with reasonably similar parameters ($\Delta EQ = 0.69$ mm s^{-1}, $\delta = 0.35$ mm s^{-1}) reported for a metakaolinite-based geopolymer treated with ferric nitrate solution [18] was suggested to be associated with some unspecified poorly crystalline ferric oxyhydroxide. Ferric doublets have been reported for nanophase ferric oxide particles, poorly crystalline ferric oxyhydroxides, Fe-bearing glasses, pyroxenes, orthopyroxenes, and clinopyroxenes [18, 24, 25, 28–34], although the parameters of none of these species conform exactly to the present ferric doublet. The poorly crystalline character of both the Fe(III) and the augite [Fe(II) site B] is evidenced by the relatively broader linewidths of these doublets by comparison with forsterite Fe(II) site A (Table 4). The broadness of the ferric doublet suggests that these sites may be associated with the amorphous component of the ashes.

Upon conversion of the ashes to geopolymers by alkali activation, the Mössbauer parameters of Fe(II) site A, assigned to ferroan forsterite, remain unchanged in both ashes, indicating that this mineral is a spectator phase and takes no part in the geopolymer-forming reaction. By contrast, a significant proportion of the Fe(II) site B, corresponding to augite, is oxidized to Fe(III) (Fig. 4; Table 4), shown by the 38 % decrease in the intensity of the Fe(II) site B of sample Va1 with a concomitant 30 % increase in Fe(III). A similar phenomenon is observed in sample Va2 in which the Fe(II) site B decreases by 21 % while the Fe(III) site intensity increases by 19 %.

These results and the changes in the Mössbauer parameters of the Fe(II) site B and Fe(III) sites upon reaction with alkali indicate that some of the octahedral ferrous sites in the augite phase of the original ashes are taking part in geopolymer formation, but although the parameters of the Fe(II) sites in augite are slightly changed after reaction with the alkali, they are still consistent with ferrous iron in octahedral sites [30, 31], albeit less distorted than in the unreacted ash. By contrast, the Mössbauer parameters of the newly formed Fe(III) sites are somewhat different from those of the ferric sites in the original ashes, showing a decrease in the isomer shifts and an increase in the quadrupole splitting (Table 4). The room-temperature isomer shifts of tetrahedral Fe^{3+} are reported to fall near or below 0.3 mm s^{-1}, whereas the isomer shifts of octahedral Fe^{3+} occur above about 0.4 mm s^{-1} [25, 29]. Thus, after alkali activation, the isomer shifts suggest a change in the Fe^{3+} coordination from sixfold to distorted sites approaching tetrahedral coordination. The Mössbauer parameters of these distorted sites are also very similar to the reported parameters of fivefold coordinated ferric sites ($\Delta EQ = 0.74$ mm s^{-1}, $\delta = 0.36$ mm s^{-1}) [28]. Either of these interpretations would provide an explanation of the observed Mössbauer parameters, and although they would tend to rule out the location of the ferric iron in the better-defined tetrahedral sites in geopolymers, they are not inconsistent with the known situation in other gels, for instance aluminosilicate gels in which 4, 5, and 6-fold Al coordination is well known to occur [35]. Thus, the ferric iron may reside in a more amorphous gel-like phase rather than in the conventional four-coordinated sites of the geopolymer structure.

These results shed light on the role of the iron minerals in the geopolymerization of volcanic ash. Previous studies on the effect of iron on this reaction have been inconclusive, probably due to differences in the form of the iron in the initial components of the geopolymer mixtures [15, 17, 18]. The geopolymer-forming reaction was suggested to be inhibited by the presence of dissolved network-forming Fe^{3+} due to its faster reaction than Si and Al to form hydroxide or oxyhydroxide phases, thereby removing OH^- ions from the solution and retarding the dissolution of the remaining aluminosilicate particles [17, 36, 37]. In another study, Fe^{3+} was suggested to contribute to geopolymer formation by entering the network structure [18]. The similarity in charge and ionic radius of Fe^{3+} and Al^{3+} has led to ferric iron in silicate glasses being considered as a network former located in a tetrahedral site [28]. Since the structure of geopolymers consists of tetrahedral aluminate and silicate units randomly linked by oxygen atoms [5–8], the decrease of the isomer shift and quadrupole splitting

of ferric iron after alkali activation may be consistent with the entry of Fe^{3+} into the geopolymer network, albeit in extremely distorted sites, or as a gel-like phase.

To summarize the Mössbauer results, one of the two crystalline Fe^{2+}-bearing mineral phases present in the original ashes, ferroan forsterite, does not participate in or interfere with the geopolymer-forming reaction, but a significant proportion of the augite present reacts with alkali to form new ferric sites with Mössbauer parameters similar to distorted tetrahedral or fivefold coordinated sites which may be located in an X-ray amorphous gel-like phase rather than in the well-defined tetrahedral network of the geopolymer product. On the other hand, if the iron was included in the amorphous geopolymer network, a simplistic chemical charge-balancing consideration would require it to be located in the tetrahedral sites. This possible inclusion in the geopolymer structure could also explain the development of strength beyond the NaO_2/Al_2O_3 ratio of 1 (Table 1). The fact that the ferrous iron in site A (ferroan forsterite) remained unaffected by alkali activation of the ashes indicates that the behavior of iron during alkali activation relies on its chemical and mineralogical state in the starting materials.

Conclusions

The presence of the crystalline iron-containing phases ferroan forsterite and augite in the present volcanic ashes does not militate against the formation of viable geopolymers with very good compressive strengths upon activation with NaOH. SEM with elemental mapping shows that iron and calcium are homogeneously distributed throughout the alkali-activated material, but the magnesium map indicates that the forsterite occurs in discrete particles.

Mössbauer spectroscopy indicates the presence of an additional ferric site in the original volcanic ashes with parameters suggesting its possible location in an X-ray amorphous octahedral environment. Upon activation with NaOH, the ferroan forsterite does not react, but a substantial number of the octahedral ferrous sites in the crystalline augite is converted to ferric sites with parameters similar to distorted tetrahedral or fivefold coordinated sites. The homogeneous distribution of iron throughout the product suggests that these new ferric sites may form part of the structural network, and may not be deleterious for the development of mechanical strength.

References

1. Barbosa VFF, MacKenzie KJD, Thaumaturgo C (2000) Int J Inorg Mater 2:309
2. Rahier H, Van Mele B, Wastiels J, (1996) J Mater Sci 31:80. doi:10.1007/BF00355129
3. Duxson P, Provis JL, Lukey GC, van Deventer JSJ (2007) Cem Concr Res 37:1590
4. Davidovits J (1991) J Therm Anal 37:1633
5. O'Connor SJ, MacKenzie KJD (2010) J Mater Sci 45:3707. doi:10.1007/s10853-010-4383-x
6. MacKenzie KJD, Rahner N, Smith ME, Wong A (2010) J Mater Sci 45:999. doi:10.1007/s10853-009-4031-5
7. Rahier H, Wastiels J, Biesemans M, Willlem R, Van Assche G, Van Mele B (2007) J Mater Sci 42:2982. doi:10.1007/s10853-006-0568-8
8. Kamseu E, Bignozzi MC, Melo UC, Leonelli C, Sglavo VM (2013) Constr Build Mater 38:1135
9. Tsai Y-L, Hanna JV, Lee Y-L, Smith ME, Chan JCC (2010) J Solid State Chem 183:3017
10. Brew DRM, MacKenzie KJD (2007) J Mater Sci 42:3990. doi:10.1007/s10853-006-0376-1
11. Waychunas GA, Kim CS, Banfield JF (2005) J Nanopart Res 7:409
12. Diaz EI, Allouche EN, Eklund S (2010) Fuel 89:992
13. Lemougna PN, MacKenzie KJD, Melo UFC (2011) Ceram Int 37:3011
14. Tchakoute Kouamo H, Mbey JA, Elimbi A, Kenne Diffo BB, Njopwouo D (2013) Ceram Int 39:1613
15. Lloyd RR, Provis JL, van Deventer JSJ (2009) J Mater Sci 44(2):608. doi:10.1007/s10853-008-3077-0
16. Provis JL, Rose V, Bernal SA, van Deventer JSJ (2009) Langmuir 25(19):11897
17. van Deventer JSJ, Provis JL, Duxson P, Lukey GC (2007) J Hazard Mater A139:506
18. Perera DS, Cashion JD, Blackford MG, Zhaoming Z, Vance ER (2007) J Eur Ceram Soc 27:2697
19. Wagh AS, Douse VE (1991) J Mater Res 6:1094
20. Kamseu E, Leonelli C, Perera DS, Melo UC, Lemougna PN (2009) Interceram 58:136
21. Bell JL, Kriven WM (2010) In: Singh D, Kriven WM (eds) Mechanical properties and performance of engineering ceramics and composites IV. Wiley, Hoboken, pp 301–312
22. Deer WA, Howie RA, Zussman J (1978) Rock-forming minerals, 2nd Ed., Volume 2A. Longman, London
23. Duxson P, Mallicoat SW, Lukey GC, Kriven WM, van Deventer JSJ (2007) Colloid Surf A Physicochem Eng Asp 292:8
24. Greenwood NN, Gibb TC (1971) Mössbauer spectroscopy, Ch 10. Chapman and Hall, London
25. Bancroft MG, Maddock AG, Burns RG (1967) Geochim Cosmochim Acta 31:2219
26. Cheong S, Ferguson P, Hermans DA, Jameson GNL, Prabkabar S, Herman DA, Tilley RD (2012) Chempluschem 77:135
27. Roca AG, Marco JF, Morales MD, Serna CJ (2007) J Phys Chem C 111:18577
28. Rossano S, Behrens H, Wilke M (2008) Phys Chem Mineral 35:77
29. Mysen BO (2006) Geochim Cosmochim Acta 70:2337
30. Spiering B, Seifert FA (1985) Contrib Miner Petrol 90:63
31. Bancroft GM, Burns RG, Stone AJ (l968) Geochim Cosmochim Acta 32: 547
32. Van Cromphaut C, de Resende VG, De Grave E, Van Alboom A, Vandenberghe RE, Klingelhöfer G (2007) Geochim Cosmochim Acta 71:4814
33. Akasaka M (1983) Phys Chem Mineral 9:205
34. Thompson A, Rancourt DG, Chadwick OA, Chorover J (2011) Geochim Cosmochim Acta 75:119
35. MacKenzie KJD, Smith ME (2002) Multinuclear solid state NMR of inorganic materials. Pergamon-Elsevier, Oxford
36. Provis JL (2006) Modelling the Formation of Geopolymers, PhD Thesis, University of Melbourne, Australia
37. Daux V, Guy C, Advocat T, Crovisier J-L, Stille P (1997) Chem Geol 142:109